

Contribution of disconnected diagrams to the hyperfine splitting of charmonium

The QCD-TARO Collaboration: Philippe de Forcrand^a, Margarita García Pérez^b, Hideo Matsufuru^c, Atsushi Nakamura^d, Irina Pushkina^e, Ion-Olimpiu Stamatescu^f, Tetsuya Takaishi^g and Takashi Umeda^h

^a*Institut für Theoretische Physik, ETH-Hönggerberg, CH-8093 Zürich, Switzerland, and Department of Physics, CERN, Theory Division, CH-1211 Geneva 23, Switzerland*
E-mail: forcrand@phys.ethz.ch

^b*Instituto de Física Teórica, Universidad Autónoma de Madrid, Cantoblanco, 28049 Madrid, Spain*
E-mail: Margarita.Garcia.Perez@cern.ch

^c*Computing Research Center, High Energy Accelerator Research Organization (KEK), Tsukuba 305-0801, Japan*
E-mail: hideo.matsufuru@kek.jp

^d*IMC, Hiroshima University, Higashi-Hiroshima 739-8521, Japan*
E-mail: nakamura@riise.hiroshima-u.ac.jp

^e*School of Biosphere Sciences, Hiroshima University, Higashi-Hiroshima 739-8521, Japan*
E-mail: irina@riise.hiroshima-u.ac.jp

^f*Institut für Theoretische Physik, Universität Heidelberg, D-69120 Heidelberg, Germany, and FEST, Schmeilweg 5, D-69118 Heidelberg, Germany*
E-mail: I.O.Stamatescu@ThPhys.Uni-Heidelberg.DE

^g*Hiroshima University of Economics, Hiroshima 731-0192, Japan*
E-mail: takaishi@hiroshima-u.ac.jp

^h*Yukawa Institute for Theoretical Physics, Kyoto University, Kyoto 606-8502, Japan*
E-mail: tumeda@yukawa.kyoto-u.ac.jp

ABSTRACT: We discuss the contribution of OZI-suppressed diagrams to the hyperfine splitting of charmonium in lattice QCD. We study valence quark mass regions from strange to charm quark masses. No contribution of the disconnected diagram is seen in the vector meson channel. In the pseudo-scalar channel and for valence quark masses around the strange quark, the disconnected contribution induces a considerable increase of the meson mass. This contribution quickly decreases as the quark mass increases. For charmonium the effect is very small although a decrease of the pseudoscalar mass induced by the disconnected contribution cannot be ruled out.

KEYWORDS: Lattice Quantum Field Theory, Lattice Gauge Field Theories, Lattice QCD.

Contents

1. Introduction	1
2. Formulation	4
2.1 Quarkonium correlation function	4
2.2 Valence quark action	4
3. Numerical simulations	5
3.1 Lattice setup	5
3.2 Tuning of valence heavy quark action	6
3.3 Connected correlators	7
3.4 Evaluation of disconnected diagram	8
3.5 Quarkonium correlators	9
4. Conclusions and discussion	12

1. Introduction

Lattice QCD has been able to provide a wealth of results for the hadron spectrum, both in the quenched approximation and with dynamical quarks [1]. Most of the low-lying hadron masses are reproduced under extrapolation to the continuum limit and to the physical u and d quark masses. Even in the quenched approximation there is a remarkable agreement with experimental data for the light hadron spectrum, deviations typically amounting to 10 per cent. The charmonium hyperfine splitting is, however, an exception to such success. Recent systematic computations in the quenched approximation have pointed out a significant discrepancy between the lattice results and experimental data: the former is 30–40% smaller than the latter, $\Delta M = M_{J/\psi} - M_{\eta_c} = 117$ MeV.

It is difficult to address the calculation of charmonium spectrum with current computational resources. Since the charm quark mass is not well below the accessible lattice cutoffs, lattice formulations that reduce the $O(am_c)$ lattice artifacts seem mandatory. The most promising, while brute force approach, is to use a relativistic formulation with sufficiently small lattice spacing and $O(a)$ -improved quark actions. This is the approach taken in Ref. [2] by the QCD-TARO Collaboration, using the nonperturbatively $O(a)$ -improved Wilson quark action on quenched isotropic lattices [2]. Numerical simulations with lattice cutoffs ranging from 2 to 5 GeV found $\Delta M = 77(2)(6)$ MeV in the continuum limit.

Other approaches involve the use of effective heavy quark actions. Among them, non-relativistic QCD (NRQCD) has been investigated most extensively. The latest NRQCD quenched result is $\Delta M = 55(5)$ MeV (with the scale set by the P - S splitting) [3]. In this

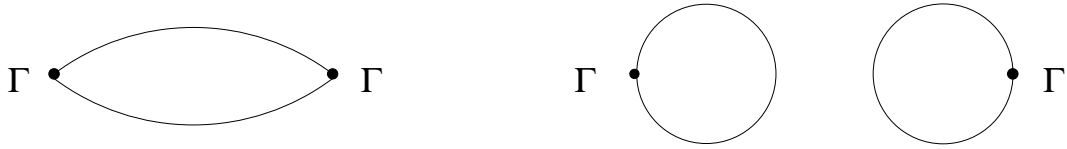


Figure 1: Connected (Left) and OZI-suppressed (Right) diagrams contributing to the pseudoscalar ($\Gamma = \gamma_5$) and vector ($\Gamma = \gamma_\mu$) channels.

case, lattice artifacts are difficult to control since brute force elimination by taking the continuum limit is impossible. Relativistic formulations, such as the Fermilab approach [4, 5] and anisotropic lattices [6, 7, 8, 9], have an advantage in this sense. However, they give results for the, continuum extrapolated, hyperfine splitting which also definitely deviate from experiment. Here it should be noted that for a quark mass not sufficiently smaller than the spatial lattice cutoff, the dynamics inside heavy quarkonia may not be precisely described by these actions whose spatial derivative terms are defined only with nearest neighbouring sites. This is because of the $O((a_\sigma p)^2)$ errors, where a_σ is the spatial lattice spacing and p the typical quark momentum. This error might become important for heavy quarkonium, for which $p \sim \alpha m_q$ [9, 10]. This is in contrast with the situation for light and heavy-light hadrons, where $p \sim \Lambda_{QCD}$. Therefore advantages of these relativistic formulations applied to heavy quarkonia are rather limited.

From all the previous studies, disagreement between the quenched lattice calculation and experiment has been established for the charmonium hyperfine splitting.

There are two candidates to explain this discrepancy. The first one is dynamical quark effects. Although a systematic study of these effects, involving a continuum extrapolation, has not been performed yet, several groups have tried to estimate them [11, 12, 13]. A recent lattice computation with 2+1 flavours of improved staggered quarks at $a^{-1} \simeq 1.6$ GeV has reported a hyperfine splitting $\Delta M = 97(2)$ GeV [13]. This value is still 20% smaller than the experimental one. Since they applied the Fermilab action with tadpole-improved tree-level value for the clover coefficient, the remaining discrepancy may be attributed to the $O(\alpha a)$ and $O((ap)^2)$ systematic errors. Systematic studies with higher lattice cutoffs and involving continuum limit extrapolations are strongly desired.

Another possible contribution, which has not been incorporated in any of the lattice computations (quenched or unquenched) performed up to now, comes from OZI-suppressed (disconnected) diagrams as those in Fig. 1 [2]. Such diagrams must be included in the evaluation of correlators of unflavoured mesons, such as η_c and J/ψ . Although, according to the perturbative picture, this contribution is expected to be small in heavy quarkonium, it might be non-negligible compared to the, also small, hyperfine splitting. Moreover, its effect might be enhanced. This happens, indeed, in the light quark mass region, where the contribution of the disconnected diagram to the pseudoscalar channel is strongly enhanced by the $U_A(1)$ anomaly ¹. It is therefore important to quantify the size of such contribution

¹Note, however, that the contribution of the $U_A(1)$ anomaly raises the mass of the pseudoscalar while not affecting that of the vector. This effect would induce a decrease of the hyperfine splitting, instead of the increase required to match the experimental value for charmonium.

to the charmonium correlator.

The goal of this paper is to examine the second possibility. A similar analysis has recently been performed by McNeile and Michael (UKQCD Collaboration) in Ref. [20]. We aim here at an exploratory study to estimate whether the disconnected diagram can give a significant contribution to the charmonium hyperfine splitting. This issue is not completely disentangled from the one of dynamical quark effects. Indeed, these effects can be particularly large for disconnected diagrams. In the quenched approximation closed quark loops, as those in the right panel of Fig. 1, can only be connected through gluonic contributions. For unquenched simulations, however, they can also be connected by insertion of virtual quark loops. This induces a very different asymptotic behaviour between quenched and unquenched disconnected correlators, as discussed at length for the case of the lattice determination of the η' mass [14]. In addition, through the disconnected diagram charmonium states mix with glueballs and lighter quarkonium. Mixing with the latter is completely neglected in the quenched calculation, while mixing with the former is only partially taken into account.

We do not intend here to analyze the failure of the quenched approximation in the calculation of the hyperfine splitting but to address the more general question of whether disconnected correlators can give a sizable contribution to this splitting. Since it is expected that such contribution will be quickly obscured by statistical noise, large statistics is essential for the present study and this has dictated our choice of lattice parameters and lattice action. The number of configurations collected for the quenched calculation of the hyperfine splitting in [2] is not sufficient for this study and increasing the statistics for these large lattices is beyond our computational resources. For this reason we use, instead, a large set (3200) of available configurations with a rather coarse $12^3 \times 24$ lattice, with fixed lattice cutoff $a^{-1} \simeq 1.2$ GeV and with two dynamical flavours of staggered quarks with $am_{\text{sea}} = 0.10$ (no attempt at a continuum extrapolation will be presented in this paper). Given the rather large sea quark masses adopted, we expect the effect of dynamical quarks to be relatively small, hence our results give also an insight for the quenched situation. It would be important to study the sea quark mass dependence to examine how such contribution shifts the charmonium masses for physical sea quark masses and $N_f = 3$.

In order to treat charm quarks on our rather coarse lattice, we adopt the Fermilab quark action. Since the disconnected diagram contribution to the charmonium hyperfine splitting is hard to detect because of large statistical noise, we also compute this contribution for lighter valence quarks, and estimate how it varies as the valence quark mass is increased towards that of the charm quark. This helps us determine its value at the charm quark mass. This is the only purpose of our varying the valence quark mass. For lighter valence quarks, the inconsistency between our sea and valence quark actions would generate systematic errors, which would cause additional problems for the determination of the meson spectrum and of the hyperfine splitting. We do not consider this regime here.

The paper is organised as follows. In the next section we describe the set up for our calculation. Section 3 presents our results. The last section is devoted to conclusions and discussion.

2. Formulation

2.1 Quarkonium correlation function

We define the quarkonia correlation function with a quarkonium operator $O(\vec{x}, t)$,

$$O(\vec{x}, t) = \sum_{\vec{y}} \bar{q}(\vec{x} + \vec{y}, t) \Gamma q(\vec{x}, t) \varphi(\vec{y}), \quad (2.1)$$

where $\varphi(\vec{y})$ is a smearing function and Γ is 4×4 matrix which specifies the quantum numbers of the quarkonium state.

We take $\Gamma = \gamma_5$ and γ_i for the pseudoscalar and vector channels, respectively. Since the operator $O(\vec{x}, t)$ contains quark fields of the same flavour, by contracting the quark lines the correlator decomposes into a connected $C_{con}(t)$ and a disconnected part $C_{dis}(t)$,

$$C_{full}(t) = \sum_{\vec{x}} \langle O^\dagger(\vec{x}, t) O(\vec{0}, 0) \rangle \equiv C_{con}(t) + C_{dis}(t). \quad (2.2)$$

Using the quark propagator $D^{-1}(\vec{x}, t; \vec{x}', t')$, where D is the Dirac operator, we can write $C_{con}(t)$ and $C_{dis}(t)$ as follows,

$$C_{con}(t) = - \sum_{\vec{x}, \vec{y}, \vec{z}} \left\langle \text{Tr} [\varphi(\vec{y}) D^{-1\dagger}(\vec{x} + \vec{y}, t; \vec{0}, 0) \gamma_5 \Gamma \varphi(\vec{z}) D^{-1}(\vec{x}, t; \vec{z}, 0) \Gamma \gamma_5] \right\rangle, \quad (2.3)$$

$$C_{dis}(t) = \frac{1}{V_3} \langle L(t)^* L(0) \rangle, \quad (2.4)$$

where Tr is the trace over the colour and spinor indices, V_3 the spatial volume. The quark loop diagram $L(t)$ is defined as

$$L(t) = \sum_{\vec{x}, \vec{y}} \text{Tr} [\varphi(\vec{y}) D^{-1}(\vec{x}, t; \vec{x} + \vec{y}, t) \Gamma]. \quad (2.5)$$

As the valence quark mass increases, the disconnected correlator is expected to decrease compared to the connected part and the extraction of a signal for the disconnected part may become increasingly difficult. It is therefore crucial to improve the quarkonium operator so as to increase the overlap with the ground state. For this purpose, we use spatially extended operators with smearing function $\varphi(\vec{x})$ in the Coulomb gauge. For $\varphi(\vec{x})$ we adopt Gaussian functions with width around the expected charmonium radius and select the best one among them.

In order to evaluate the trace in Eq. (2.5), we employ the complex Z_2 noise method [16]. This method is a popular technique to evaluate quark loop contributions to correlators. An application to the smeared operator, Eq. (2.5), is straightforward. We note that one needs to solve the quark propagator only once for each noise vector for all the smearing functions applied.

2.2 Valence quark action

The coarse lattice we employ does not allow for an isotropic formulation of heavy valence quarks whose mass is not sufficiently smaller than the lattice cutoff. For this reason we

adopt the Fermilab action [4],

$$\begin{aligned}
S_q = \sum_{x,y} \bar{q}(x) \left\{ \delta_{xy} - \kappa_\sigma \gamma_F \left[(1-\gamma_4)U_4(x)\delta_{x+\hat{4},y} + (1+\gamma_4)U_4(x-\hat{4})\delta_{x-\hat{4},y} \right] \right. \\
- \kappa_\sigma \sum_i \left[(r-\gamma_i)U_i(x)\delta_{x+\hat{i},y} + (r+\gamma_i)U_i(x-\hat{i})\delta_{x-\hat{i},y} \right] \\
\left. - \kappa_\sigma c_E \sum_i \sigma_{4i} F_{4i}(x,y)\delta_{x,y} - \kappa_\sigma c_B \sum_{i>j} \sigma_{ij} F_{ij}(x,y)\delta_{x,y} \right\} q(y), \tag{2.6}
\end{aligned}$$

where the spatial Wilson parameter is set to $r = 1$. The parameter γ_F is to be tuned so that the rest mass, $M_1 \equiv E(\vec{p} = 0)$, equals the kinetic mass,

$$\frac{1}{M_2} \equiv \left. \frac{\partial^2 E(\vec{p})}{\partial p_i^2} \right|_{\vec{p}=0}, \tag{2.7}$$

for, for example, a meson dispersion relation. We define κ by incorporating tadpole improvement [17] as

$$\frac{1}{\kappa} \equiv \frac{1}{u_0 \kappa_\sigma} - 2(\gamma_F + 3r - 4) \quad (= 2(m_0 + 4)), \tag{2.8}$$

where m_0 is the bare quark mass [18]. As the mean-field value of link variable, u_0 , we adopt the average value in the Landau gauge, $u_0 = \langle \text{Tr} U_\mu(x) \rangle / 3$. The value of γ_F is tuned for each value of κ . Then the chiral extrapolation is to be performed in $1/\kappa$, a step that is not taken in this paper. The clover coefficients, c_E and c_B , control the $O(a)$ systematic uncertainty. In this work, we adopt the tadpole improved values [17],

$$c_E = c_B = 1/u_0^3. \tag{2.9}$$

This action allows, in principle, for a relativistic treatment of heavy quarks but, as pointed out in Sec. 1, even with nonperturbatively tuned γ_F , the results suffer from $O((ap)^2)$ errors, where $p \sim \alpha m_q$ in the case of heavy quarkonium, in addition to the $O(\alpha a)$ error from the clover terms. We expect this effect not to be essential for a qualitative estimate of the size of the contribution from the disconnected diagram. Better control over these errors is required, however, for a quantitative evaluation and continuum extrapolation of the contribution.

3. Numerical simulations

3.1 Lattice setup

The numerical simulation is performed on lattices of size $12^3 \times 24$, with two flavours of staggered dynamical quarks. The gauge action is the standard Wilson plaquette action with $\beta = 5.50$. The dynamical staggered quark mass is $m_{sea} a = 0.10$. The configuration is generated with the hybrid R-algorithm with $\delta t = 0.02$ and unit length of trajectory. We prepare 32 independent initial configurations and generate configurations in parallel. Each configuration is separated by 5 trajectories, after 900 trajectories for thermalization.

The lattice cutoff scale is set by Sommer's hadronic radius, r_0 , which is defined through $r_0^2 F(r_0) = 1.65$, where $F(r)$ is the force between static quark and antiquark [19]. Setting

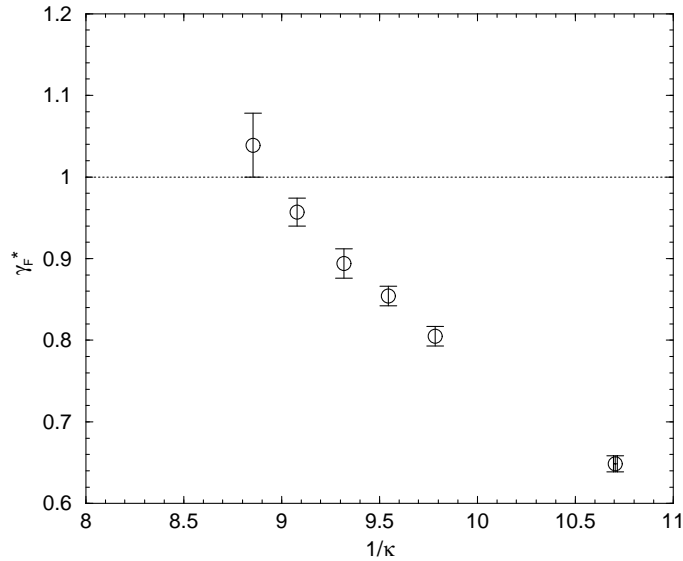


Figure 2: Tuned parameter γ_F^* using the meson dispersion relation.

κ	γ_F^*	N_{conf}	N_{NV}	$m_{PS}a$	m_Va
0.11294	1.039	1920	50	0.60714(92)	0.8479(17)
0.11013	0.957	1920	100	0.90071(81)	1.0753(13)
0.10732	0.894	1920	100	1.17518(74)	1.3135(11)
0.10476	0.854	1920	150	1.41022(70)	1.5257(10)
0.10220	0.805	3200	300	1.65156(51)	1.75154(73)
0.093417	0.6485	3200	300	2.50132(48)	2.56858(61)

Table 1: Parameters of the valence quarks. N_{conf} is the number of gauge configurations used; they are generated from 32 independent initial configurations. The pseudoscalar and vector meson masses are extracted from connected correlators with smeared operators.

$r_0 = 0.5$ fm yields $a^{-1} = 1.2012(60)$ GeV. For tadpole improvement [17], the mean-field value is determined in the Landau gauge as $u_0 = \langle \text{Tr} U_\mu(x) \rangle / 3$, giving $u_0 = 0.824285(89)$ and clover coefficient $c_{SW} = 1.785$ for our lattice. In the following analysis, the statistical error is estimated by the jackknife method.

3.2 Tuning of valence heavy quark action

In this subsection, we describe the tuning of the parameter γ_F in the valence quark action. The tuning procedure is the same as for anisotropic lattices [18]. At each hopping parameter κ , the coefficient γ_F in the quark action (2.6) is determined nonperturbatively using the meson dispersion relation. For the meson dispersion relation, we assume the relativistic form

$$E(\vec{p})^2 = M_1^2 + \frac{M_1}{M_2} \vec{p}^2 + O(\vec{p}^4), \quad (3.1)$$

where M_1 and M_2 are the rest and kinetic masses of the meson. The value of γ_F is tuned so that $M_1 = M_2$ holds.

The tuning of γ_F is performed with connected correlators of point operators, namely $\varphi(\vec{x}) = \delta(\vec{x})$, on 400 configurations. The meson energies are fitted to a quadratic form for the pseudoscalar and vector channels. The obtained $\xi_F = \sqrt{M_2/M_1}$, the fermionic anisotropy, are spin averaged and fitted to a linear function of γ_F . Interpolating to $(M_1/M_2) = 1$, the tuned value of γ_F, γ_F^* , is determined.

The result for γ_F^* is displayed in Fig. 2. Since in the light quark mass region the Fermilab action smoothly tends to the standard clover quark action, the value of γ_F^* should approach unity as the quark mass decreases. From a tree level analysis, it should be a decreasing function of $1/\kappa$, and in the light quark mass region, a linear dependence in m_q^2 is expected ($m_q = (1/\kappa - 1/\kappa_c)/2$, where κ_c is the critical hopping parameter (which is not determined on the present lattice). In Fig. 2, although the decreasing tendency as $1/\kappa$ increases is indeed observed, the quark mass dependence in the small mass region seems not in agreement with the expected behaviour. This is presumably due to large lattice spacing artifacts, one of which apparently comes from the assumed form of the meson dispersion relation. This uncertainty may also cause γ_F^* to approach a value slightly different from unity [18]. Although we will not try to correct these systematic errors for the present qualitative estimate of the hyperfine splitting, it is essential to have them under control in order to extract reliable quantitative determinations.

The value of κ corresponding to the charm quark mass is determined by interpolating the results for the vector meson mass so as to reproduce the physical J/ψ meson mass. The value of γ_F^* is also interpolated to that κ value. The resulting κ and γ_F^* are listed in the last line of Table 1, and displayed as the rightmost point in Fig. 2 together with the other five cases listed in Table 1.

3.3 Connected correlators

Charmonium correlators are computed for the quark parameters listed in Table 1. Let us start with the connected correlator, Eq. (2.3). In the following analysis, the error due to the uncertainty in γ_F^* is not evaluated.

We first observe the efficiency of the smearing technique on the connected correlators. Figure 3 displays the effective mass plot for the connected correlators with local and smeared operators in pseudoscalar and vector channels. Here the effective mass is defined with

$$\frac{C(t)}{C(t+1)} \equiv \frac{\cosh [(T/2 - t)m_{eff}(t)]}{\cosh [(T/2 - t - 1)m_{eff}(t)]}. \quad (3.2)$$

We use smearing functions with Gaussian form and several width values, and select the one that gives better plateaus in the effective mass plot. Figure 3 clearly shows that the smeared operator considerably enhances the overlap with the ground state, which dominates the connected correlator beyond $t = 4$.

In Table 1 we list the meson masses extracted from the connected correlators. At the charm quark mass, the obtained hyperfine splitting, $\Delta M \simeq 81$ MeV, is consistent with previous results [13], and again far below the experimental value.

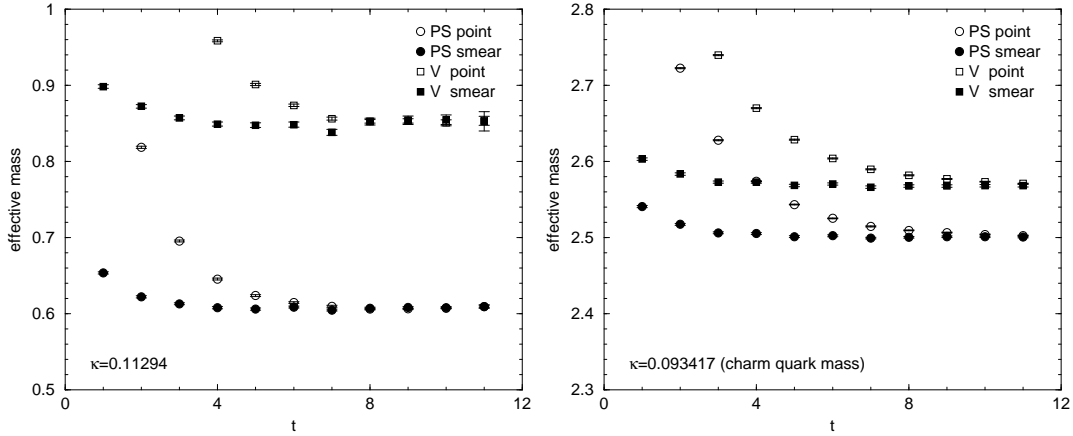


Figure 3: Effective masses of connected correlators with local and smeared operators.

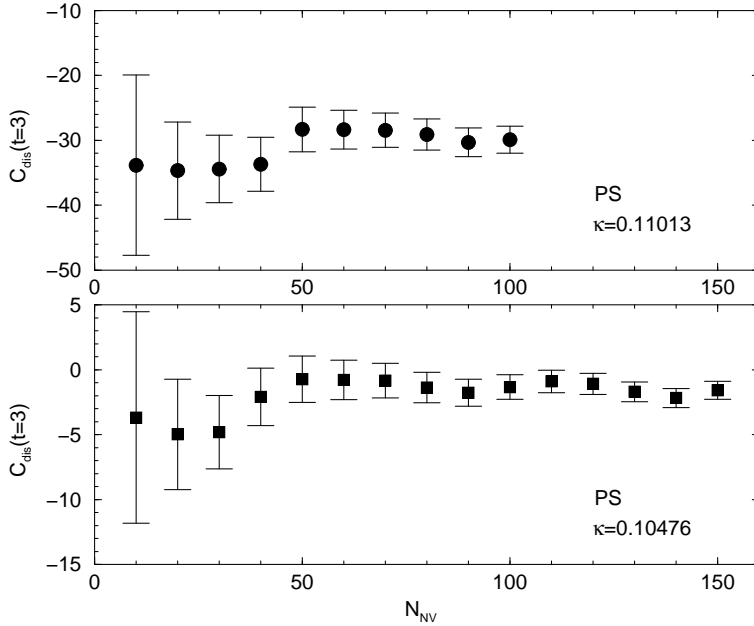


Figure 4: Typical samples of the dependence on the number of noise vector of pseudoscalar disconnected correlators at $t = 3$. Since the results are averaged over configurations, the error includes both that of the noise method and that of the ensemble average.

3.4 Evaluation of disconnected diagram

For an evaluation of the disconnected correlators, Eq. (2.4), we apply the Z_2 noise method. Figure 4 shows typical samples of the pseudoscalar disconnected correlator at a time slice $t = 3$ as a function of the number of noise vectors. The top and bottom panels display the results for $\kappa = 0.11013$ and 0.10476 . Since the results are ensemble averages over configurations, the displayed error includes both the quantum fluctuations and the error due to a finite number of noise vectors.

In order to estimate the contribution of disconnected diagrams we have to control both errors. A reasonable approach is to choose the number of noise vectors, N_{NV} , so as

to keep both errors at similar levels. Although we can find an “optimal N_{NV} ” at each t by observing N_{NV} dependence of the error displayed in Fig. 4, it is sufficient to roughly estimate such N_{NV} , since increasing the number of configurations, N_{conf} , also reduces the error of noise method and we choose rather large values of N_{conf} . The number of noise vectors, N_{NV} , and gauge configurations, N_{conf} selected for each valence quark mass are displayed in Table 1. As the quark mass increases, the signal to noise ratio becomes worse rapidly. Thus a larger number of configurations as well as of noise vectors are prepared in this calculation.

3.5 Quarkonium correlators

In this section we evaluate the relevance of the disconnected part of the meson correlator for the meson spectrum. Figs. 5 and 6 show the ratio $R(t) = C_{dis}(t)/C_{con}(t)$. $R(t)$ is often used to evaluate the contribution of the disconnected diagram [15]. If the ground state dominates both the connected and full correlators, their asymptotic time dependence can be described by single exponentials:

$$C_{con}(t) = A_{con} \exp(-m_{con}t), \quad (3.3)$$

$$C_{full}(t) = C_{con}(t) + C_{dis}(t) = A_{full} \exp(-m_{full}t). \quad (3.4)$$

Then the ratio behaves as

$$R(t) = \frac{C_{dis}(t)}{C_{con}(t)} = \frac{A_{full}}{A_{con}} \exp\{-(m_{full} - m_{con})t\} - 1. \quad (3.5)$$

This ratio is useful for exploring the sign and magnitude of the mass difference ($m_{full} - m_{con}$) when the signal is noisy. In Figs. 5 and 6, we plot both point and smeared correlator ratios $R(t)$. For the latter, effective masses for full and connected correlators are also displayed in the right panels of Figs. 5 and 6.

For the vector channel, we find no sizable contribution from the disconnected diagram in the whole quark mass region explored. Similar results have been also reported in [15]. This is consistent with the OZI suppression. In contrast, in the pseudoscalar channel, a clear signal is observed in the light quark mass region giving rise to an increase of the pseudoscalar mass. This is consistent with previous works on the flavour singlet η (η') meson and with theoretical expectations. It is important to note that this effect is opposite to what would be needed to match the experimental result for charmonium. Given that the vector mass receives no sizable contribution, a decrease of the η_c mass by about 30–40 MeV is required to bring the lattice measurement of the hyperfine splitting up to the value of 117 MeV measured in experiment. Indeed, the mass difference between full and connected correlators rapidly decreases as the quark mass increases, leaving in principle room for a change in the sign of the mass difference. In the left bottom panel of Fig. 6, the dashed curves represent $R(t)$ from Eq. 3.5 for $m_{full} - m_{con} = \pm 20$ MeV, assuming $A_{full}/A_{con} = 1$. In the scale of the plot, a small deviation of A_{full}/A_{con} from one would induce a shift of the curves, keeping the slopes almost constant. Due to the large statistical errors for $t > 2$ we cannot make any definite statement about the slope of the data: it is compatible with zero within errors but small slopes of order ± 20 MeV cannot be ruled out.

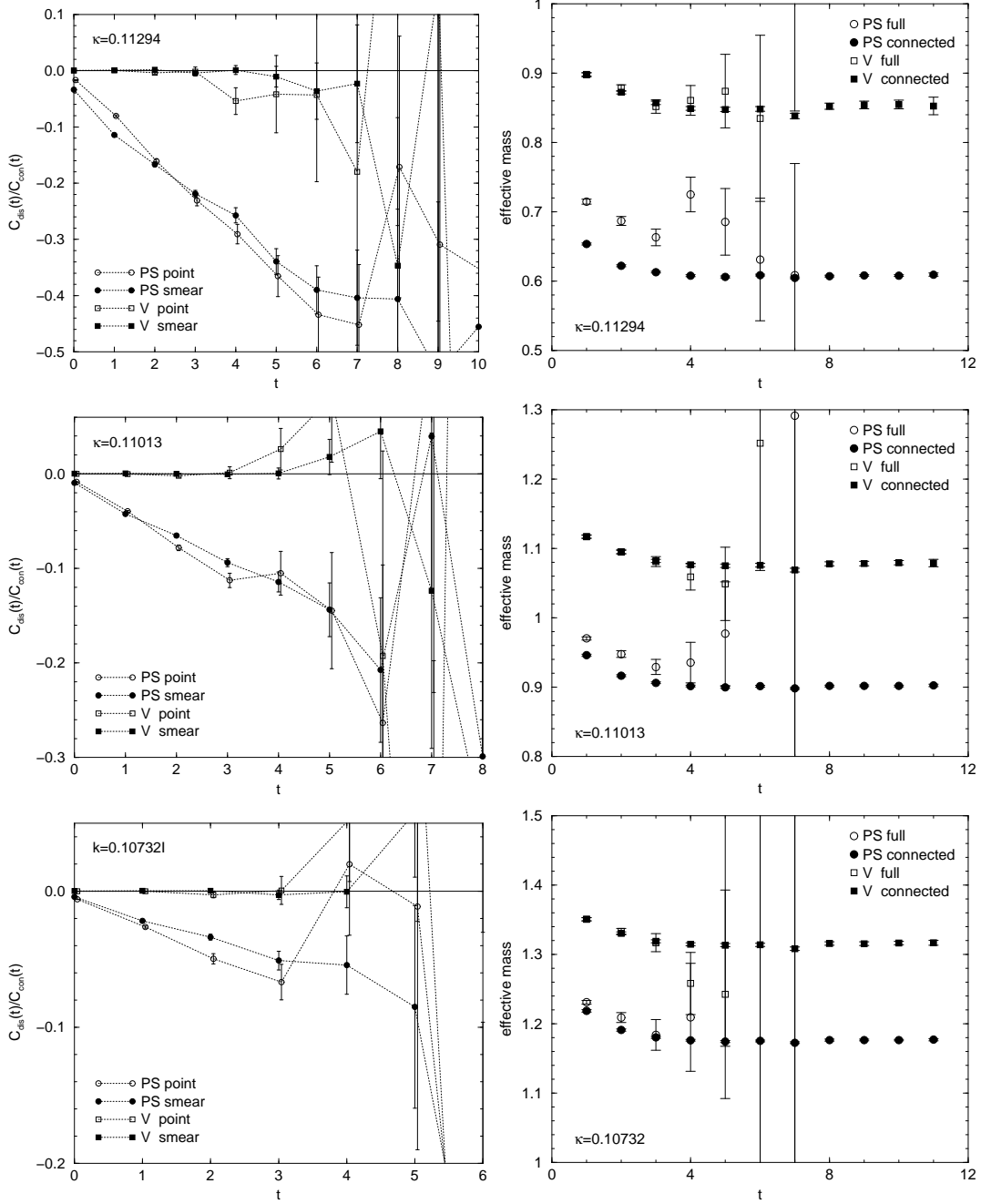


Figure 5: Ratio of disconnected to connected correlators (left panels) and effective mass of full and connected correlators (right panels) for $\kappa = 0.11294$ (top), 0.11013 (middle), and 0.10732 (bottom).

To better settle this point, we plot in Fig. 7 the mass difference between the full and connected correlators for the pseudoscalar channel as a function of the vector meson mass. Here the mass difference is defined by the difference between effective masses of full and connected correlators at $t = 1$ and $t = 2$. At these time slices, the effective mass plots in Figs. 5 and 6 do not exhibit clear plateau behaviour. However, the contribution of the excited states partially cancel in the difference. In fact, the results for $t = 1$ and 2 differ

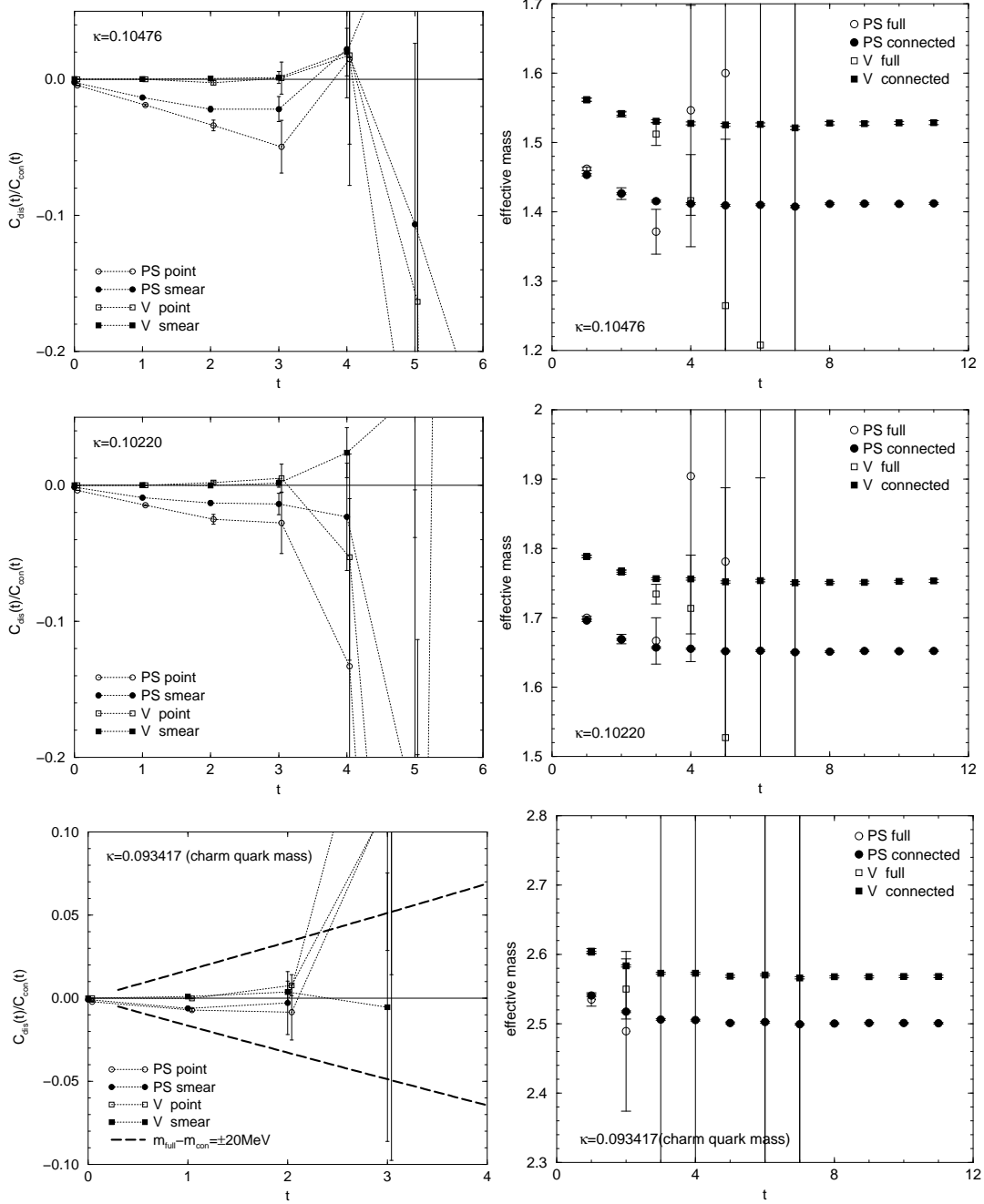


Figure 6: The same quantities as Fig. 5 for $\kappa = 0.10476$ (top), 0.10220 (middle) and 0.093417 (bottom). The latter value of κ corresponds to the charm quark. In the left bottom panel, the dashed curves represents the cases where $m_{\text{full}} - m_{\text{con}} = \pm 20 \text{ MeV}$ with $A_{\text{full}}/A_{\text{con}} = 1$.

from each other only slightly. We do not plot the result for $t = 2$ at the charm quark mass because the result is too noisy. Figure 7 again shows that the mass difference between full and connected correlator is positive for light quark masses. It rapidly decreases as the quark mass increases, becoming almost zero at about half the charm quark mass. Our results at the charm quark mass are not conclusive. At the one sigma level they are compatible both

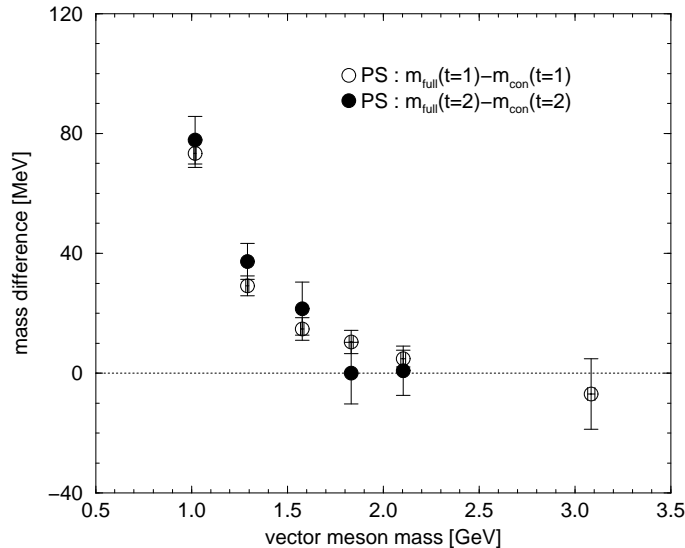


Figure 7: The mass difference between the full and connected correlators, in the pseudoscalar channel, defined with the effective masses at $t = 1$ and $t = 2$ as a function of vector meson mass. We call the effective mass at "t = 1" that derived from comparing $t = 2$ and $t = 1$.

with zero mass difference or with a negative mass difference of about -20 MeV. This is consistent with the results found by McNeile and Michael (UKQCD Collaboration) in [20].

4. Conclusions and discussion

We have investigated the contribution of disconnected diagrams to the hyperfine splitting of quarkonium in a quark mass region ranging from strange to charm quark masses. As displayed in Figures 5, 6, we found almost no contribution of disconnected diagrams to the correlators in the vector channel in the whole quark mass region explored in this work. For the pseudoscalar channel, however, there is a sizable contribution around the strange quark mass region which quickly decreases as the quark mass increases and almost vanishes around half the charm quark mass. At the charm quark mass, the contribution of the disconnected correlator is very small, in agreement with the expected OZI suppression. Given our large statistical errors we cannot, however, rule out that the mass difference between full and connected correlators becomes negative, although small. In this respect we agree with the results previously found by McNeile and Michael [20] who found room for a mass difference of the order of -20 MeV.

To determine how large is the contribution of disconnected diagrams for more physical situations, one needs to perform the chiral extrapolation in the sea quarks and the continuum limit. As argued in the introduction, going to lighter sea quarks may considerably modify the contribution from disconnected diagrams. In particular, an effect that could induce a further decrease in the η_c mass would be mixing with a pseudoscalar glueball were this to be lighter than the η_c . This is a possibility that has been discussed also in [20], although it has been considered not very likely given the fact that lattice determinations of the pseudoscalar glueball gives masses below that of the η_c meson.

Acknowledgements

The numerical simulations were done using a Hitachi SR8000 at the High Energy Accelerator Research Organization (KEK), and a NEC SX-5 at the Research Center for Nuclear Physics, Osaka University. It should be noted that the success of simulation owes also to a gigabit network, SuperSINET supported by National Institute of Informatics, for efficient and timely data transfer. H. M. and T. U. were supported by the Japan Society for the Promotion of Science for Young Scientists. M.G.P. has been supported by a Ramón y Cajal contract of the MCyT.

References

- [1] For a recent review, see e.g. C. McNeile, arXiv:hep-lat/0307027.
- [2] S. Choe et al. [QCD-TARO Collaboration], *J. High Energy Phys.* **08** (2003) 022 [arXiv:hep-lat/0307004].
- [3] H. D. Trottier, *Phys. Rev.* **D 55** (1997) 6844 [arXiv:hep-lat/9611026]. N. H. Shakespeare and H. D. Trottier, *Phys. Rev.* **D 58** (1998) 034502 [arXiv:hep-lat/9802038].
- [4] A. X. El-Khadra, A. S. Kronfeld and P. B. Mackenzie, *Phys. Rev.* **D 55** (1997) 3933 [arXiv:hep-lat/9604004].
- [5] S. Aoki, Y. Kuramashi and S. i. Tominaga, *Prog. Theor. Phys.* **109** (2003) 383 [arXiv:hep-lat/0107009].
- [6] T. R. Klassen, *Nucl. Phys.* **73** (*Proc. Suppl.*) (1999) 918 [arXiv:hep-lat/9809174].
- [7] P. Chen, *Phys. Rev.* **D 64** (2001) 034509 [arXiv:hep-lat/0006019]. P. Chen, X. Liao and T. Manke, *Nucl. Phys.* **94** (*Proc. Suppl.*) (2001) 342 [arXiv:hep-lat/0010069].
- [8] T. Umeda, R. Katayama, O. Miyamura and H. Matsufuru, *Int. J. Mod. Phys.* **A 16** (2001) 2215 [arXiv:hep-lat/0011085].
- [9] CP-PACS Collaboration (A. Ali Khan et al.), *Nucl. Phys.* **94** (*Proc. Suppl.*) (2001) 325 [arXiv:hep-lat/0011005];
CP-PACS Collaboration (M. Okamoto et al.), *Phys. Rev.* **D 65** (2002) 094508 [arXiv:hep-lat/0112020].
- [10] J. Harada, H. Matsufuru, T. Onogi and A. Sugita, *Phys. Rev.* **D 66** (2002) 014509 [arXiv:hep-lat/0203025].
- [11] C. Stewart and R. Koniuk, *Phys. Rev.* **D 63** (2001) 054503 [arXiv:hep-lat/0005024].
- [12] A. X. El-Khadra, S. Gottlieb, A. S. Kronfeld, P. B. Mackenzie and J. N. Simone, *Nucl. Phys.* **83** (*Proc. Suppl.*) (2000) 283.
- [13] M. Di Pierro *et al.*, arXiv:hep-lat/0310042, *Nucl. Phys.* **119** (*Proc. Suppl.*) (2003) 586 [arXiv:hep-lat/0210051].
- [14] For a review see S. Gusken, “Flavor singlet phenomena in lattice QCD,” arXiv:hep-lat/9906034.
- [15] C. McNeile, C. Michael and K. J. Sharkey [UKQCD Collaboration], *Phys. Rev.* **D 65** (2002) 014508 [arXiv:hep-lat/0107003].

- [16] S.-J. Dong and K.-F. Liu, *Phys. Lett.* **B 328** (1994) 130 [arXiv:hep-lat/9308015].
- [17] G. P. Lepage and P. B. Mackenzie, *Phys. Rev.* **D 48** (1993) 2250 [arXiv:hep-lat/9209022].
- [18] H. Matsufuru, T. Onogi and T. Umeda, *Phys. Rev.* **D 64** (2001) 114503 [arXiv:hep-lat/0107001].
- [19] R. Sommer, *Nucl. Phys.* **B 411** (1994) 839 [arXiv:hep-lat/9310022].
- [20] C. McNeile and C. Michael [UKQCD Collaboration], arXiv:hep-lat/0402012.

